Available online at www.sciencedirect.com
ScienceDirect
Journal of the European Ceramic Society 31 (2011) 673–685
www.elsevier.com/locate/jeurceramsoc

Influence of body composition on the technological properties and mineralogy of stoneware: A DOE and mineralogical–microstructural study

Magdalena Lassinantti Gualtieri [a,*], Marcello Romagnoli [a], Alessandro F. Gualtieri [b]

[a] *Dipartimento Ingegneria dei Materiali e dell'Ambiente, Università degli studi di Modena e Reggio Emilia, Via Vignolese 905/a, I-41100 Modena, Italy*
[b] *Dipartimento di Scienze della Terra, Università degli studi di Modena e Reggio Emilia, I-41100 Modena, Italy*

Received 1 October 2010; received in revised form 29 November 2010; accepted 2 December 2010
Available online 3 January 2011

Abstract

This paper reports a systematic and comprehensive investigation of the effects of the starting mixture composition on the mineralogy and properties of porcelain stoneware tiles using mixture design and full quantitative phase analyses by the Rietveld method. Functional relationships between properties and the raw material mixture proportions were obtained and related to the mineralogical composition of the fired product. Mullite crystallisation depended on the chemical environment. Dissolved quartz mounted to 10 wt% of the dry body regardless on initial amount, indicating saturation of the surrounding melt. The paramount role of the amorphous content on the stoneware properties was disclosed quantitatively. Open porosity decreased with increasing amount of amorphous content, and consequently both the stain and wear resistance increased. The CIE-Lab colour parameters a^* and b^* increased with increased amorphous content due to interaction with surface iron in hematite. The mullite content increased wear resistance, thus supporting the mullite strengthening theory.

Keywords: Sintering; Microstructure-final; Porcelain; Stoneware tile; Design of Experiment

1. Introduction

Stoneware tiles are the foundation of the ceramic industry due to high technological performance and outstanding aesthetic appearance.[1] The typical raw materials used to formulate a stoneware body are quartz, feldspars and clays. However, due to limited natural sources of conventional raw materials, efforts in research have been made to introduce secondary raw materials [2–8] and non-conventional or poor raw materials.[9] Replacement of traditional raw materials with other components in order to improve the technological properties of the fired product has also been extensively investigated.[10–13]

The production process of porcelain stoneware is rather simple, including wet grinding of raw material mixtures, preparation of slip and spray drying of the slip which results in humid (ca. 6 wt% moisture) powder aggregates. The powder is uniaxially pressed and subsequently fired in a fast firing cycle (ca. 1 h) with a maximum temperature in the range 1190–1230 °C. The final product is composed of a mixture of crystalline phases (newly formed mullite and residual quartz and feldspar) and glass.[5] The partial replacement of conventional raw materials may lead to the crystallisation of additional high-temperature phases.[5,8] During the firing process, a sequence of intercrystalline (regarding a single crystalline/amorphous phase) and extracrystalline (interaction of a crystalline/amorphous phase with another) reactions take place[14]: (a) dehydroxylation of clay minerals and the consequent formation of pseudo-amorphous products (such as metakaolinite from kaolinite dehydroxilate product); (b) crystallisation of primary mullite from pseudo-amorphous products with a consequent segregation of a silica rich amorphous phase; (c) formation of an alkaline melt originating from the melting of feldspar; (d) viscous sintering, or vitrification, in which the viscous melt fills up the pores in the body under the influence of capillary forces so that a dense body is obtained; (e) partial decomposition of quartz due to instability in the presence of the alkaline melt; (f) crystallisation of secondary mullite.

The technological properties of stoneware tiles such as water absorption, mechanical properties, frost resistance, chemical resistance and stain resistance are governed by the material's

* Corresponding author. Tel.: +39 059 2056282; fax: +39 059 2056243.
E-mail address: magdalena.gualtieri@unimore.it (M. Lassinantti Gualtieri).

0955-2219/$ – see front matter © 2010 Elsevier Ltd. All rights reserved.
doi:10.1016/j.jeurceramsoc.2010.12.002

Table 1
Mineralogical composition of the raw materials as determined by XRPD data and Rietveld refinements.

Raw material	Mineralogical composition (wt%)						
	Quartz	K-feldspar	Plagioclase	Kaolinite	Anatase	Muscovite-illite	Smectite
A	18.1 (5)	–	76.0 (4)	2.7 (4)	–	3.2 (7)	–
B	27.4 (2)	–	–	69.6 (2)	–	3.0 (4)	–
C	14.9 (2)	1.8 (3)	1.2 (2)	65.5 (5)	0.7 (2)	9.4 (6)	6.5 (8)
D	100	–	–	–	–	–	–

microstructure, the porosity in particular, which in turn is dependent on the starting composition.[15] Although a myriad of studies regarding microstructural and functional properties of stoneware tiles have been reported,[10,11,15–27] a complete picture of the effect of raw material mixtures on the microstructure and technological properties is difficult to obtain due to the complex interchange between raw materials as well as a high dependence on the firing kinetics.[24,28] The major component of porcelain stoneware tiles is glass and a proper quantification of this phase should be important for a full understanding of the system. A suitable technique for this purpose is quantitative phase analysis using the Rietveld method,[29,30] which allows to quantitatively determine both the crystalline and amorphous fractions. This methodology is increasingly used for the microstructural characterisation of porcelain stoneware.[4,12,13,28,29,31]

The complex reaction pathways taking place during firing of porcelain stoneware may involve synergistic or competitive effects between raw materials which are difficult to identify using traditional experimental approaches. These problems can be resolved using Mixture Design[32] which is a type of Design of Experiment (DOE) method. In DOE, experiments are properly distributed within a factor space in order to minimise the number of experiments required to obtain a statistically valid functional relationship between a response and factors. In a mixture design, the factors are the proportions of a mixture. Data are analysed by regression methods and the validity of the results is evaluated using statistics such as goodness of fit (R^2), goodness of prediction (Q^2), analysis of variance (ANOVA) and normal probability plots.[33] A final validation of the statistical models can be performed using a number of test compositions. In traditional ceramics, mixture design has been used to tailor the composition of different ceramic systems such as ceramic powders,[34] clay bricks,[35] glazes and frits,[36–38] synthetic pigments[39] and ceramic tiles.[19,20,36,40–43] Correia et al. compared the results from the statistical modeling with microstructural information extracted from qualitative X-ray powder diffraction (XRPD) analyses and scanning electron microscopy (SEM) analyses.[40,41] However, a full quantification of the mineralogical composition of the fired products was not performed. In recent studies, De Noni et al. used mixture design to relate the starting composition of porcelain tile with the developed phases during firing and the mechanical properties of the samples.[19,20]

The present work is aimed to provide a comprehensive picture of the raw materials effect on the mineralogical composition and various technological properties (total porosity, linear firing shrinkage, stain resistance, resistance to deep abrasion, whiteness and bulk density) of the fired product using fixed process conditions. Mixture design and statistical modeling were combined with microstructural information extracted from SEM analyses and full quantitative phase analyses using XRPD data and the Rietveld method. This investigation will help to further contribute to the full understanding of the fast-fired stoneware tile system in terms of mineral assemblages and microstructure.

2. Materials and methods

The investigated raw materials, commonly used for the industrial manufacture of stoneware tiles, are: (A) sodium feldspar, (B) kaolin, (C) kaolinite-illite rich clay and (D) quartz sand. The stoneware tile samples were prepared in such a way as to reproduce common industrial conditions as follows: each mixture was wet milled for 20 min in an alumina jar using a solid:liquid ratio of 1.5 and alumina balls as grinding media. A fluidiser (Reoflux 30/70 Lamberti Ceramic Additives srl) was added to improve the rheology of the slurry (0.1 wt%). Following milling, the suspension was dried at 110 °C and the resulting powder was deagglomerated and humidified (6 wt%). A fixed amount of humidified powder (25 g) was dry pressed (515 kg/cm^2) into a disc with a diameter of 40 mm. Five discs from each mixture were prepared. The as-prepared bodies were dried at 110 °C for 24 h followed by firing in an electric kiln at a maximum firing temperature of 1220 °C using a heating/cooling rate of 5 °C/min and a plateau at maximum temperature of 5 min. The firing temperature was chosen based on preliminary experiments

Table 2
Chemical composition of the raw materials, determined by XRF.

Raw material	Chemical composition (wt%)								
	SiO_2	Al_2O_3	Fe_2O_3	TiO_2	CaO	MgO	Na_2O	K_2O	L.O.I.
A	70.50	17.90	0.12	0.27	0.57	0.07	9.95	0.26	0.36
B	57.6	30.7	0.66	0.28	0.23	0.01	–	0.42	10.1
C	57.2	28.2	1.1	0.6	0.54	1.0	0.15	0.79	10.5
D	99.7	0.10	0.03	0.04	0.02	0.001	0.07	0.03	0.01

in which the linear firing shrinkage was followed as a function of temperature.

X-ray powder diffraction (XRPD) data were collected using a θ/θ diffractometer (PANalytical, CuKα radiation), equipped with a real time multiple strip (RTMS) detector. Divergence and anti-scattering slits of 0.125° and 0.25°, respectively, were mounted in the incident beam pathway. The pathway of the diffracted beam included a Ni filter, a soller slit (0.02 rad) and an antiscatter blade (5 mm). A virtual step scan (0.0167° 2θ) was performed in the range 3–80° 2θ. Samples were carefully ground and mounted in aluminum sample holders using the side-loading technique. Quantitative phase analyses were performed using XRPD data and Rietveld refinements. The refinements were accomplished with the GSAS package[44] and its graphical interface EXPGUI.[45] As a large amount of glass phase is expected to be present in the stoneware tile samples, the quantitative phase analysis method using Rietveld refinements was combined with the internal standard method.[30] 10 wt% corundum (NIST 676a) was added in samples of fired products as internal standard and included in the refinements. The refined weight fractions of the crystalline phases were rescaled with respect to the known weight fraction of added standard in order to obtain the real crystalline phase weight fractions. Consequently, the glass content could be calculated.[30]

The microstructure of fired bodies was investigated using a Philips XL-40 scanning electron microscopy (SEM), equipped with an energy dispersive X-ray fluorescence spectrometer (EDS). The surface structure was observed on as-fired samples, whereas bulk observations were performed on polished samples (embedded in epoxy resin). The samples were mounted on aluminum stubs and gold coated (ca. 10 nm thin layers).

Chemical analyses of raw materials were performed using X-ray fluorescence spectroscopy (XRF, Philips PW 1480).

The linear firing shrinkage was calculated using the formula $((L_g - L_f)/L_g) \times 100$, where L_g and L_f are the mean diameter of the dry and the fired discs, respectively.

The CIE-Lab colour parameters (L^*, a^* and b^*) of fired samples were determined using a COROB-Colour Engineering spectrophotometer with optical geometry d/8, illuminant D65 and observer 10°.

The functional surface staining of fired samples was evaluated using methylene blue as staining agent (aqueous solution, 10 g/l). The sample surface was subjected to the staining agent for 24 h after which the samples were carefully washed under running water and dried. The amount of staining agent retained by the surface after washing was quantified by ΔE^* which is calculated according to the following formula:

$$\Delta E* = \sqrt{\Delta L*^2 + \Delta a*^2 + \Delta b*^2}$$

where ΔL^*, Δa^* and Δb^* are the difference between the colour parameters L^*, a^* and b^*, before and after staining.

Deep abrasion tests of fired samples were performed according to EN ISO 10545.7 using an abrasimeter (Ceramic Instrument AP/87). The diameter of the rotating steel disc was 200.1 mm and alumina grains (FEPA 80) were used as abrasive medium. The number of revolutions was limited to 40 so that the trace would not exceed the sample border. The volume of material removed by abrasion (V_{ab}) was calculated according to the following formula:

$$V_{ab} = \left(\frac{\pi\alpha}{180} - \sin\alpha\right)\frac{hd^2}{8}$$

where $\sin(\alpha/2) = l/d$, l is the length of trace, d and h are the diameter and thickness, respectively, of the rotating disc.

A GeoPyc 1360 Envelope and T.A.P. Density Analyzer (Micromeritics Inc., USA) was used to determine the bulk density of the fired samples (ρ_b).

The true density (ρ_t) of the fired samples was determined using a gas displacement pycnometer instrument (AccuPyc 1330, Micromeritics Inc., USA). The total porosity (TP) was calculated according to:

$$\mathrm{TP} = \left(1 - \frac{\rho_b}{\rho_t}\right) \times 100$$

The dry bulk density (ρ_{db}) was determined, after drying at 24 h at 110 °C, using the weight and the dimensions which were carefully determined using an analytical balance and a micrometer, respectively.

A D-optimal mixture design, accomplished using the software Design-Expert v. 6.0.10 (Stat-ease Inc.), was utilised to define the raw material mixtures for the preparation of the stoneware bodies. The same software was used in consequent data analyses. Constraints were set on the component proportions, so that the proportions of the raw material were only allowed within limited ranges. These ranges were set to 20–60, 5–40, 5–25, and 0–25 wt% for raw materials A, B, C and D, respectively. Statistically relevant regression models, connecting the raw material proportions to the measured properties (i.e. TP, LFS, ΔE^*, V_{ab}, L^* and ρ_b), were obtained using analysis of variance (ANOVA). For final verification of the applicability of the statistical models, a test set of five compositions, different from the ones defined by the design but within the experimental domain, was prepared and evaluated.

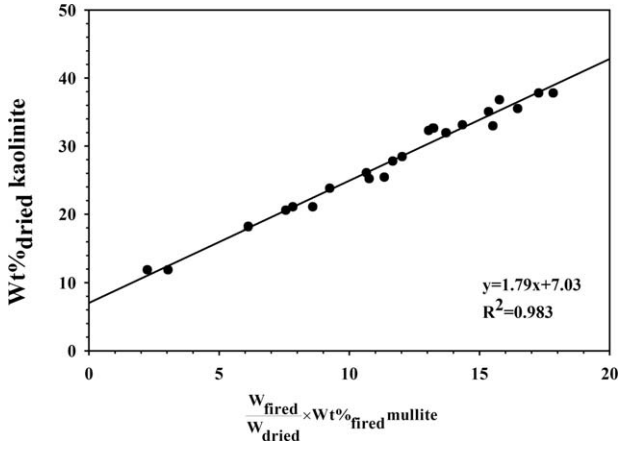

Fig. 1. The wt% of kaolinite in the dried body (calculated based on the mineralogical composition of the raw materials and their proportions in the mixture) as a function of the wt% mullite multiplied by the fired/dried absolute weight of the ceramic body.

3. Results and discussion

3.1. Characterisation of the raw materials

The mineralogical and chemical composition of the raw materials used for the preparation of the stoneware tile samples are shown in Tables 1 and 2, respectively. The agreement factors of the Rietveld refinements for quantitative phase analyses (QPA), as defined in GSAS[44] were in the ranges $R_p = 0.057–0.089$, $R_{wp} = 0.076–0.117$ and $\chi^2 = 1.82–2.27$.

3.2. Statistical analyses and model evaluation

Table 3 reports the composition of the body formulations under investigation, defined by a D-optimal mixture design, as well as the experimental results for the dry bulk density and various properties of the fired samples. Based on the experimental results, statistically valid mathematical models were obtained that relate measured properties of the fired stoneware tile with the proportions of the raw materials. These models were used to obtain Design-Expert constant contour plots, presented in a later section, which graphically demonstrate the net effect of the raw materials on the investigated properties of the fired product. The equations, as well as the model statistics, are available upon request to the corresponding author. To counter-check the statistical models, five test specimens were prepared and evaluated. The raw material compositions of these samples are shown in Table 4, together with measured/predicted properties. There is a high accordance between the experimental and predicted values, which is mirrored in high linear regression coefficients (predicted vs. experimental), see Table 4. In fact, the probability to obtain such high values for uncorrelated data is less than 0.6%.[46] In addition, the regression line invariably lies within the error bars of each property.

3.3. Effect of raw materials on the phase composition of the fired sample

Results from quantitative phase analyses of the fired products are displayed in Table 5. The agreement factors of the refinement, as defined in GSAS[44] were in the ranges $R_p = 0.041–0.064$, $R_{wp} = 0.051–0.091$ and $\chi^2 = 1.18–3.6$. The main component of the fired samples is the amorphous phase. The crystalline fraction is composed of residual quartz and feldspar in addition to newly formed mullite.

The QPA analyses using the Rietveld method also provide accurate values of the unit cell parameters of mullite which can be used to obtain information regarding the crystal structure and chemical composition.[47,48] The latter parameter is difficult to obtain with high accuracy using electron microscopy in combination with energy dispersive spectroscopy (EDS) analyses due to limited spatial resolution.[49] It is well-known that mullite may form solid solutions with cations of transition metals such as Fe, with a consequent increase in the unit cell parameters.[50] Considering that the raw material mixtures contain Fe, it was speculated that some Fe could have been incorporated in the mullite structure and that a correlation could exist between the

Table 3
Mixture composition (wt%) and experimental results for dry bulk density (ρ_{db}), total porosity (TP), staining resistance defined by ΔE^*, volume of material removed by abrasion (V_{ab}), fired bulk density (ρ_b), true density (ρ_t), linear firing shrinkage (LFS) and the CIE-Lab colour parameters (L^*, a^*, b^*). Mean of 4–5 samples is reported together with the 95% confidence interval.

Mix	Run	A	B	C	D	ρ_{db} (g/cm^3)	TP (%)	ΔE^*	V_{ab} (mm^3)	ρ_b (g/cm^3)	ρ_t (g/cm^3)	LFS (%)	L^*	a^*	b^*
5	1	45	5	25	25	2.02 ± 0.01	8 ± 2	39 ± 2	49 ± 11	2.35 ± 0.06	2.544 ± 0.007	5.8 ± 0.2	81.3 ± 0.6	1.9 ± 0.1	9.6 ± 0.1
2	2	55	40	5	0	1.962 ± 0.007	7 ± 1	6 ± 4	48 ± 4	2.36 ± 0.02	2.53 ± 0.01	7.5 ± 0.1	80.7 ± 0.5	2.2 ± 0.2	9.9 ± 0.3
16	3	20	30	25	25	2.035 ± 0.007	20 ± 2	59 ± 2	75 ± 12	2.1 ± 0.04	2.62 ± 0.02	3.6 ± 0.3	92.0 ± 0.3	0.7 ± 0.1	6.5 ± 0.2
6	4	60	5	20	15	1.97 ± 0.01	8 ± 1	9 ± 1	54 ± 3	2.31 ± 0.02	2.50 ± 0.01	6.0 ± 0.1	76.1 ± 0.3	2.8 ± 0.2	11.65 ± 0.06
4	5	39.167	21.667	14.167	25	2.00 ± 0.01	13 ± 2	53 ± 3	80 ± 5	2.22 ± 0.04	2.561 ± 0.003	4.8 ± 0.3	87.2 ± 0.5	1.4 ± 0.1	8.0 ± 0.1
10	6	35	40	25	0	2.028 ± 0.009	8 ± 2	40 ± 5	42 ± 2	2.37 ± 0.04	2.57 ± 0.02	6.93 ± 0.08	86.9 ± 0.5	1.0 ± 0.2	8.8 ± 0.1
17	7	55	40	5	0	1.94 ± 0.01	6.5 ± 0.7	5 ± 4	45 ± 4	2.37 ± 0.01	2.54 ± 0.01	7.9 ± 0.2	80.9 ± 0.7	2.1 ± 0.3	10.0 ± 0.2
13	8	31.875	32.708	18.125	17.292	2.01 ± 0.02	15 ± 2	55 ± 3	58 ± 6	2.2 ± 0.04	2.59 ± 0.01	5.1 ± 0.5	90.1 ± 0.7	1.0 ± 0.1	7.1 ± 0.4
20	9	30	40	5	25	1.926 ± 0.003	21 ± 3	58 ± 5.0	128 ± 22	2.05 ± 0.05	2.59 ± 0.02	3.4 ± 0.5	91.9 ± 0.3	0.9 ± 0.1	5.5 ± 0.2
15	10	49.375	15.208	18.125	17.292	2.03 ± 0.04	7 ± 1	32 ± 6	48 ± 7	2.35 ± 0.02	2.54 ± 0.01	6.2 ± 0.2	81.2 ± 0.5	1.8 ± 0.2	9.7 ± 0.6
8	11	60	10	5	25	1.85 ± 0.01	6 ± 2	38 ± 2	58 ± 7	2.35 ± 0.04	2.51 ± 0.01	8.1 ± 0.1	79.6 ± 0.9	2.4 ± 0.3	10.3 ± 0.4
14	12	47.5	27.5	25	0	2.05 ± 0.01	6 ± 1	4 ± 2	42 ± 5	2.41 ± 0.04	2.55 ± 0.008	6.6 ± 0.1	78.9 ± 0.6	1.8 ± 0.2	10.5 ± 0.1
7	13	60	15	25	0	2.05 ± 0.02	7 ± 4	2 ± 1	49 ± 3	2.34 ± 0.10	2.519 ± 0.003	5.8 ± 0.1	75.8 ± 0.3	2.4 ± 0.2	10.3 ± 0.1
12	14	42.5	40	5	12.5	1.933 ± 0.005	11 ± 1	51 ± 5	63 ± 5	2.28 ± 0.01	2.56 ± 0.02	6.9 ± 0.5	88 ± 1	1.23 ± 0.04	7.7 ± 0.5
19	15	60	10	5	25	1.83 ± 0.01	7 ± 1	31 ± 4	58 ± 3	2.34 ± 0.03	2.51 ± 0.01	8.2 ± 0.1	78.6 ± 0.3	2.5 ± 0.1	10.7 ± 0.4
18	16	45	5	25	25	2.02 ± 0.04	9 ± 1	46 ± 2	65 ± 4	2.3 ± 0.04	2.54 ± 0.02	5.2 ± 0.1	83.8 ± 0.6	1.5 ± 0.1	8.9 ± 0.1
9	17	40	22.5	25	12.5	2.05 ± 0.03	10 ± 2	46 ± 3	49 ± 4	2.31 ± 0.06	2.56 ± 0.01	5.7 ± 0.2	85 ± 1	1.34 ± 0.08	9.7 ± 0.2
1	18	20	30	25	25	2.015 ± 0.005	22 ± 2	59 ± 6	99 ± 18	2.05 ± 0.05	2.619 ± 0.006	3.2 ± 0.3	93.1 ± 0.3	0.6 ± 0.1	5.6 ± 0.4
11	19	60	22.5	5	12.5	1.90 ± 0.01	6 ± 2	13 ± 3	50 ± 8	2.36 ± 0.01	2.52 ± 0.04	7.7 ± 0.1	81 ± 1	2.01 ± 0.09	9.7 ± 0.5
3	20	30	40	5	25	1.951 ± 0.004	20 ± 4	56 ± 5	125 ± 8	2.07 ± 0.09	2.60 ± 0.01	3.8 ± 0.2	92.1 ± 0.3	0.87 ± 0.05	5.4 ± 0.1

Table 4
Mixture composition (wt%) and experimental/predicted values for test set used for validation of mathematical models connecting some measured properties with proportions of raw materials (see caption of Table 3 for explanation of abbreviations). The 95% confidence interval is also given. In addition, the linear regression coefficient (predicted vs. experimental) for each sample is also included to further demonstrate the high accordance between experimental and predicted values.

Mixture	A	B	C	D	TP (%)	ΔE^*	V_{ab} (cm^3)	ρ_b (g/cm^3)	ρ_t (g/cm^3)	LFS (%)	L^*	R^2
21	52	26	10	12	6.3 ± 1.0/7.6 ± 0.6	28.5 ± 5.1/31 ± 5	52.7 ± 3.4/53 ± 3	2.36 ± 0.03/2.34 ± 0.01	2.524 ± 0.008/2.539 ± 0.002	6.84 ± 0.06/6.9 ± 0.2	81.4 ± 0.4/81.9 ± 0.6	0.999
22	56	17	22	5	5.5 ± 0.6/6.6 ± 0.8	4.6 ± 0.9/9 ± 5	47.8 ± 3.5/47 ± 4	2.38 ± 0.01/2.36 ± 0.02	2.52 ± 0.02/2.531 ± 0.003	6.24 ± 0.06/6.2 ± 0.3	79.3 ± 0.2/77.8 ± 0.9	0.997
23	28	37	13	22	19.2 ± 2.8/18.9 ± 0.8	58.2 ± 1.6/57 ± 5	82.4 ± 6.8/92 ± 15	2.11 ± 0.01/2.10 ± 0.02	2.61 ± 0.02/2.602 ± 0.004	3.76 ± 0.25/4.2 ± 0.3	91.6 ± 0.2/91.8 ± 0.9	0.994
24	41	12	24	23	11.7 ± 1.7/9.9 ± 0.9	49.1 ± 2.8/48 ± 6	66.1 ± 7.5/56 ± 6	2.26 ± 0.02/2.30 ± 0.02	2.56 ± 0.02/2.562 ± 0.003	5.00 ± 0.24/5.1 ± 0.2	86.2 ± 0.8/84.2 ± 0.8	0.992
25	46	38	8	8	8.2 ± 1.9/9.0 ± 0.7	41.2 ± 9.2/41 ± 5	54.1 ± 5.6/54 ± 4	2.35 ± 0.07/2.32 ± 0.00	2.55 ± 0.01/2.558 ± 0.004	6.86 ± 0.14/6.9 ± 0.2	85.6 ± 1.1/84.8 ± 0.8	0.996

mullite unit cell parameters and iron content. However, no such correlation was found in this work. In fact, the unit cell parameters were rather similar for all samples ($a = 7.553 \pm 0.002$; $b = 7.702 \pm 0.005$ and $c = 2.8852 \pm 0.0007$) and comparable to those found for the iron-free sample prepared at 1200 °C and reported by Ocaña et al. (i.e. $a = 7.553$ (2); $b = 7.686$ (2) and $c = 2.8850$ (8)).[50] Hence, it is probable that the mullite crystallised in the stoneware tiles studied here does not contain structural iron. This result may have important implications on the interpretation of the CIE-Lab colour parameters measured for the stoneware tile samples, and discussed later in Section 3.4.

According to Ban and Okada,[47] the mol% Al_2O_3 of mullite is related to the length of the *a*-axis (nm) according to the following empirical expression:

$$Al_2O_3\,(\text{mol\%}) = 1443 \times a - 1028.06$$

According to this equation, the mullite crystals in our samples contain 61.8 ± 0.3 mol% Al_2O_3. Hence, the mullite crystallised in our system is close to the so-called "stoichiometric" 3:2 mullite ($3Al_2O_3{\cdot}2SiO_2$). This is in full accordance with the results obtained by Paganini et al. for sanitaryware.[51]

Fig. 1 shows the wt% kaolinite in the dried body, calculated on the basis of the mineralogical composition of the raw materials and their proportions in the mixture, as a function of the wt% mullite multiplied by the fired/dried absolute weight of the ceramic body. The conversion factor applied to the wt% mullite is necessary in order to compensate for the weight loss during firing and thus render it comparable to the wt% kaolinite in the dried body. A linear dependence between kaolinite and mullite is observed, indicating that the mullite formed in our system is mainly of primary nature.[52,53] It is interesting to note that, extrapolating the linear curve, no mullite should be found when the dried bodies contain less than ca. 7 wt% kaolinite. Under these conditions, the chemical environment is undersaturated with aluminum which leads to a complete dissolution of the kaolinite relicts in the glass matrix. Another important observation, also reported by other authors,[19,26] is that the fraction of kaolinite transformed into mullite varies between 23 and 45 wt% from low to high kaolinite content which is considerably lower than the theoretical value of 54%. These observations indicate that the crystallisation of mullite from kaolinite is highly governed by the chemical composition of the liquid melt, and is accompanied by the formation of amorphous aluminosilicate. Martín-Márquez et al. stated that the incomplete conversion of kaolinite to mullite is mainly due to the fast-firing process.[28]

Fig. 2 shows the wt% quartz in the original mixture, calculated based on the raw material compositions and their proportions in the mixture, as a function of the quartz content in the fired body. The latter was renormalised to the weight of the dried body so a direct comparison is possible. A linear curve with a regression coefficient of 0.983 is obtained (<0.05% probability for uncorrelated data),[46] with the intercept of 10.3. That is, quartz contents less than 10.3 wt% in the dry body leads to a complete engulfment of the crystals in the liquid melt during

Table 5
Mineralogical composition of the stoneware bodies, prepared using the raw material mixtures defined by DOE (mixtures 1–20, see Table 3 as well as a test set of mixtures different from those defined by the design (see Table 4).

Mixture	Mineralogical composition (wt%)					
	Quartz	K-feldspar	Hematite	Mullite	Plagioclase	Amorphous phase
5	30.2 (3)	0.05 (15)	0.005 (35)	8.9 (3)	0.4 (1)	60.4 (4)
2	12.1 (1)	0.3 (1)	0.01 (3)	13.9 (2)	0.84 (8)	72.8 (3)
16	36.3 (4)	0.3 (1)	0.03 (3)	18.3 (3)	0.7 (1)	44.3 (6)
6	20.7 (2)	0.5 (1)	0.04 (3)	6.3 (2)	0.7 (1)	71.8 (3)
4	33.3 (3)	0.3 (1)	0.02 (3)	11.8 (3)	1.0 (1)	53.5 (5)
10	15.4 (2)	0.7 (1)	[a]	22.9 (3)	0.5 (1)	60.5 (3)
17	12.6 (1)	0.70 (8)	[a]	13.9 (2)	0.5 (8)	72.2 (2)
13	29.2 (3)	0.2 (1)	[a]	17.4 (3)	0.7 (1)	52.4 (5)
20	36.3 (4)	[a]	[a]	14.4 (3)	1.6 (1)	47.6 (5)
15	25.4 (2)	0.7 (1)	0.01 (3)	9.6 (2)	0.6 (1)	63.7 (4)
8	29.8 (4)	[a]	0.03 (4)	3.1 (3)	2.1 (1)	64.9 (5)
14	11.5 (1)	0.8 (1)	0.01 (3)	16.7 (2)	0.5 (1)	70.5 (3)
7	10.1 (1)	0.6 (1)	[a]	12.6 (2)	0.6 (1)	76.0 (2)
12	24.4 (2)	0.5 (1)	[a]	13.7 (2)	1.6 (1)	59.9 (4)
19	32.7 (4)	[a]	0.08 (4)	3.29 (5)	1.8 (1)	62.2 (5)
18	30.7 (4)	[a]	0.02 (4)	8.1 (3)	1.1 (2)	60.1 (5)
9	22.2 (2)	[a]	0.02 (4)	15.1 (2)	0.5 (1)	62.3 (3)
1	37.0 (5)	[a]	0.06 (4)	18.9 (4)	0.7 (1)	43.3 (6)
11	22.1 (2)	0.8 (1)	[a]	7.8 (2)	1.9 (1)	67.3 (3)
3	35.8 (4)	0.4 (1)	[a]	14.4 (3)	1.5 (3)	47.9 (5)
21	21.7 (2)	0.5 (1)	[a]	11.1 (2)	1.1 (1)	65.6 (3)
22	14.1 (1)	0.5 (1)	[a]	12.2 (2)	1.1 (1)	72.0 (3)
23	34.4 (4)	0.2 (1)	[a]	16.2 (3)	0.7 (1)	48.5 (5)
24	29.8 (3)	0.4 (2)	0.05 (3)	11.2 (3)	1.0 (1)	57.6 (4)
25	21.1 (2)	0.7 (1)	[a]	16.3 (2)	1.4 (1)	60.5 (4)

[a] Below detection limit.

firing. Increasing the quartz content in the dry body does not lead to a much higher quartz dissolution (note that the slope of the linear curve in Fig. 2 is close to one) which indicates saturation of the surrounding melt, i.e. dissolution of the quartz crystals is controlled by their chemical environment. Based on these observations, it can be assumed that the average grain size of the residual quartz crystals increases with increasing amount of quartz in the dry body. Sánchez et al. found that 64–85% of the quartz in the starting composition remained undissolved.[15] In accordance with the results presented here, a linear relation between the quartz content in the dry and fired body was also found.[15,26]

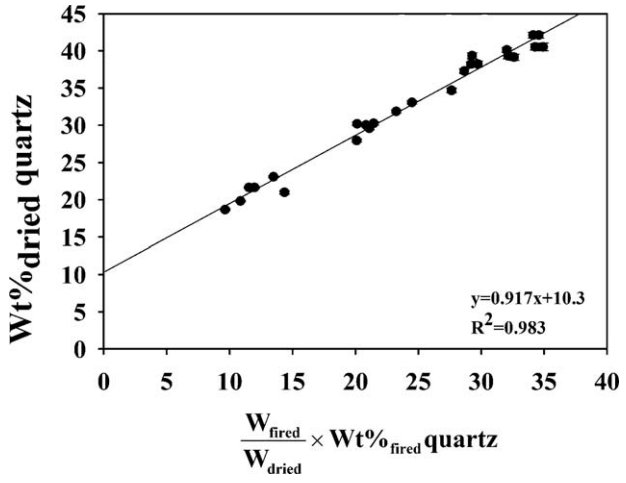

Fig. 2. The wt% quartz in the dried body, calculated based on the raw material compositions and their proportions in the mixture, versus the quartz content in the fired body. The latter was renormalized to the weight of the dried body so a direct comparison is possible.

The viscosity of the glass melt is of major importance for the microstructure development of porcelain stoneware tiles during firing. A liquid phase of low viscosity better fills up pores and voids. In addition, gases trapped in the viscous melt can escape more easily. Calculation of the chemical composition of the overall glass phase, based on the chemical analyses of the raw materials and the quantitative phase analyses of the fired samples may help to make a qualitative approximation of the viscosity of the liquid aluminosilicate melt.[54] However, it should be kept in mind that this type of discussion is highly approximate as the glass phase cannot be considered homogeneous as the contributions from feldspar, quartz and kaolinite are at least partly segregated.[19] The concentration of $K_2O + Na_2O$, which should be most indicative for the viscosity of the melt,[54] has a negative effect on viscosity. A linear decrease of the concentration of these alkali oxides in the glass phase of the fired stoneware tile was found with increasing amount of clay minerals in the starting composition ($R^2 = 0.725$). Instead a positive trend was found between alkali oxide content and feldspar ($R^2 = 0.873$). No correlation was found with quartz content, probably as the amount of dissolved quartz is independent on quartz content in the initial mixture (see Fig. 2).

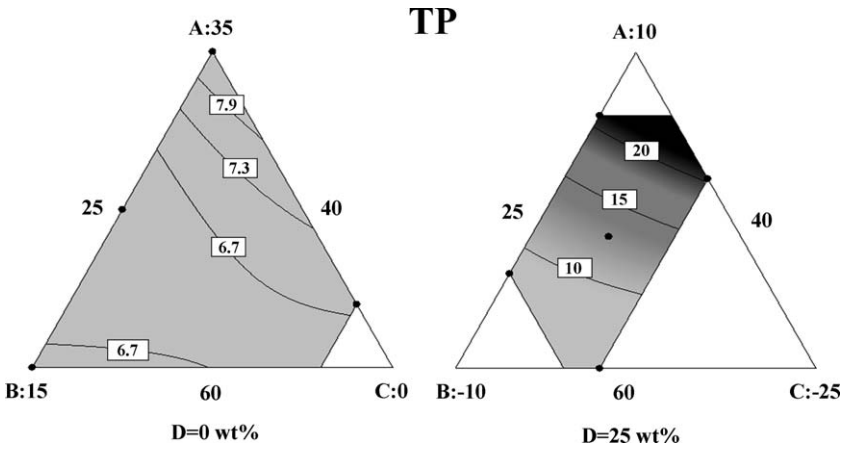

Fig. 3. Constant contour plots at low (0 wt%) and high (25 wt%) percentage of quartz sand for TP (total porosity). The raw material codes A, B, C and D correspond to feldspar, kaolin, kaolinitic-illitic clay and quartz sand, respectively.

3.4. Mineralogical composition and technological properties

The net effect of raw materials on various properties (i.e. TP, ΔE, V_{ab}, ρ_a, LFS and L^*) of the fired products is graphically demonstrated in Design-Expert constant contour plots drawn using the regression equations obtained by statistical modeling. A contour plot is a two-dimensional representation of 3D data, in which data points giving the same response value are joined to form so-called contour lines. Often, the regions between contour lines are shaded/coloured to indicate their magnitude, which helps to read the different values of the dependent variable.

As the design involves four mixture components, one component must be set as constant in each plot. It was chosen to display the contour plots at low (0 wt%) and high (25 wt%) concentration of added quartz sand (component D) for each property. The plots corresponding to each property will be discussed one by one below.

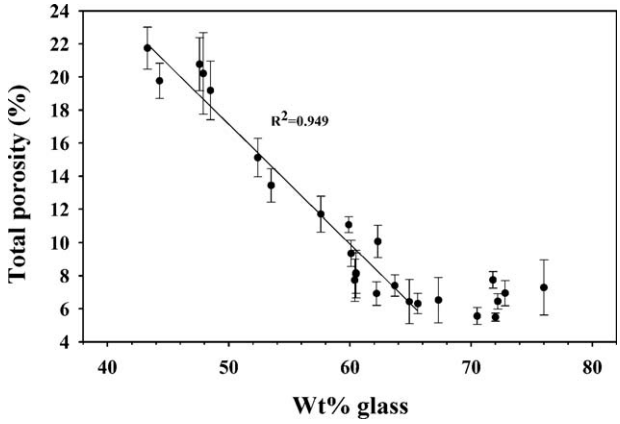

Fig. 4. Total porosity (TP, %) as a function of wt% glass in the fired body.

3.4.1. Total porosity (TP), fired bulk density (ρ_b)

The pore structure in porcelain stoneware tile is one of the most important physical properties which determines the overall characteristics of the product. The sintering process is dependent on the viscosity of the melt which in turn, in case of fixed temperature cycle, is dependent on the chemical composition.[55,56]

Fig. 3 shows the constant contour plots at low (0 wt%) and high (25 wt%) concentration of added quartz sand for TP. Very similar plots were obtained for the fired bulk density and therefore not shown here. In fact, fired bulk density is linearly

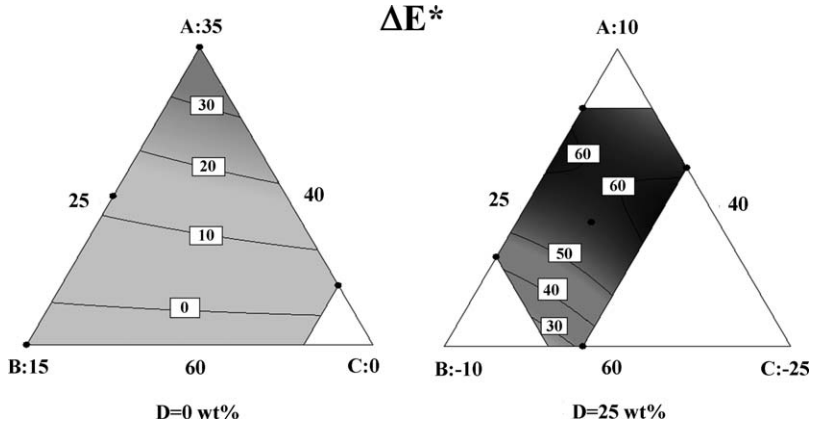

Fig. 5. Constant contour plots at low (0 wt%) and high (25 wt%) percentage of quartz sand for ΔE^*. The raw material codes A, B, C and D correspond to feldspar, kaolin, kaolinitic-illitic clay and quartz sand, respectively.

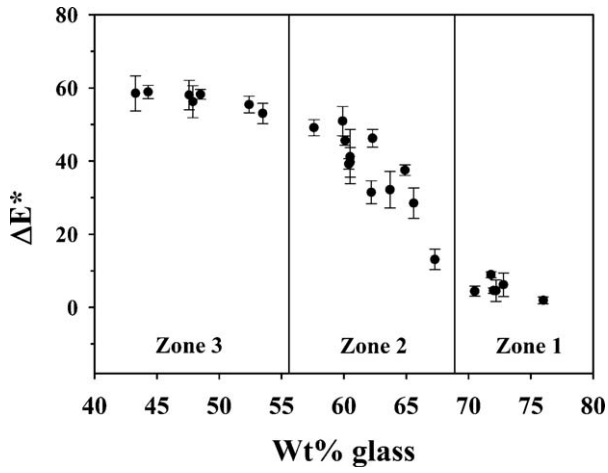

Fig. 6. ΔE^* as a function of wt% glass in the fired body. The curve can be divided in three different zones based on the slope.

correlated to total porosity with a correlation coefficient of 0.98. The probability that twenty observations between two variables with this correlation coefficient are actually uncorrelated is less than 0.05%.[46] The feldspar content strongly decreases the porosity. This is expected as viscous sintering, i.e. densification, is promoted by feldspar. In addition, the concentration of alkali oxides in the overall liquid melt (approximated from chemical and mineralogical analyses of the raw materials and the fired stoneware, see Section 3.3) increases with increasing feldspar content, thus rendering the liquid melt less viscous which speeds up the sintering process. The opposite effect is observed for quartz and kaolin. The negative effect of quartz and kaolin on total porosity observed here can be explained on the basis of previous microstructural studies performed on porcelain stoneware.[9,21] In the early stage of firing, pores are formed due to dehydroxylation reactions resulting in a more

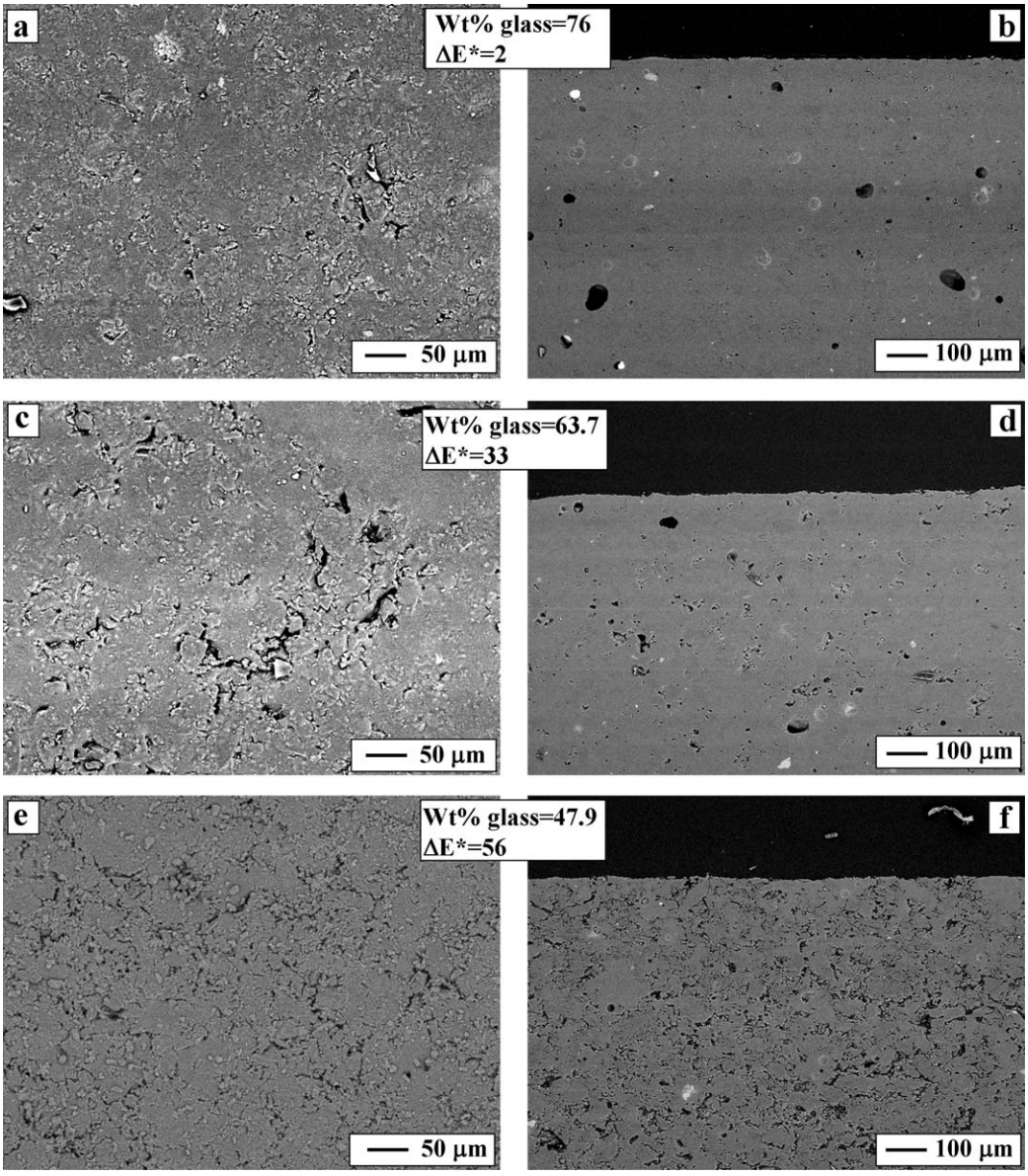

Fig. 7. Top and side view BSE images of samples with different values of ΔE^*, prepared from mixtures 7 (a and b), 15 (c and d) and 3 (e and f).

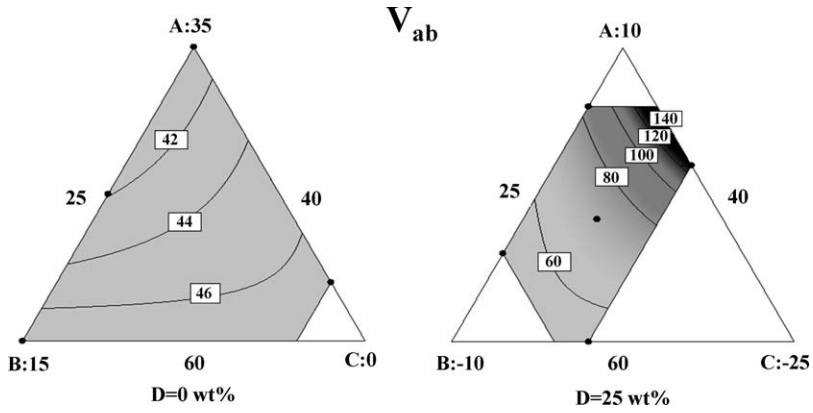

Fig. 8. Constant contour plots at low (0 wt%) and high (25 wt%) percentage of quartz sand for V_{ab}. The raw material codes A, B, C and D correspond to feldspar, kaolin, kaolinitic-illitic clay and quartz sand, respectively.

porous structure compared to the dry body.[21] These pores have to be filled by the viscous melt in order to form a dense body. Coarse quartz grains introduce larger voids in the dry compact which are difficult to eliminate by viscous sintering.[9] In fact, constant contour plots at low (0 wt%) and high (25 wt%) concentration of added quartz sand for dry bulk density (not shown here), showed that an increased amount of quartz resulted in a decrease in dry bulk density. An effect of kaolin on the viscosity of the glass melt is also expected, based on the estimation of the chemical composition of the glass phase (see end of Section 3.3). The viscosity of the liquid melt should increase with increasing content of kaolinite, thus slowing down the sintering process. This explanation is also in concert with the increased temperature of maximum density with increasing kaolinite content observed by De Noni et al.[19]

Fig. 4 shows the total porosity as a function of glass content in the fired body. A very strong dependence between the two parameters is observed, in accordance with the model that foresees an important effect of the feldspar content on total porosity. Perhaps the most interesting observation is that the curve flattens out at amorphous contents higher than about 66%. That is, higher amounts of liquid phase do not result in a more sintered body. An explanation to this observation could be the presence of gas bubbles entrapped in the liquid phase which cannot be eliminated by viscous sintering, thus forming closed pores which contribute to total porosity.

3.4.2. Amount of staining agent retained by the surface (ΔE^*)

Fig. 5 shows the constant contour plots at low (0 wt%) and high (25 wt%) concentration of added quartz sand for ΔE^*. A decrease in ΔE^* is observed with increasing amount of feldspar. On the contrary, quartz and kaolin have a positive effect on ΔE^*. These trends are qualitatively the same as the ones found for the TP (compare with Fig. 3), but not strictly correlated. In fact, Dondi et al. showed that the penetration of staining agent, and a consequent increase in ΔE^*, is manly determined by the pore structure rather than the total porosity.[17] Sánchez et al. studies polished porcelain tiles with different microstructure, obtained by varying the peak firing temperature.[15] They found that ΔE^* increased with increasing porosity at firing temperatures lower than the temperature of minimum porosity. However, at higher temperatures which represent overfiring conditions, the ΔE^* did not increase as much as porosity. This was explained by the fact that the pore structure had changed from irregular, interconnected pores to isolated round pores which are easier to clean. The kaolinite-illite clay seems to have a positive effect on ΔE^* only at low quartz content, an observation which requires further studies to be explained adequately.

Fig. 6 shows the wt% glass in the fired body versus ΔE^*. The curve can be divided in three different zones by the slope of the curve. No significant change in ΔE^* can be observed at low and high glass content (zone 3 and 1, respectively). At intermediate glass content (zone 2), ΔE^* decreases linearly with glass content. At low glass content (zone 3), the density of interconnected pores is so high that a difference in colour between samples in this zone is hardly detected due to colour saturation. In zone 2, the density of interconnected pores is low enough to reveal a decrease in ΔE^* with increasing glass content due to a decrease in open porosity contributing to total porosity

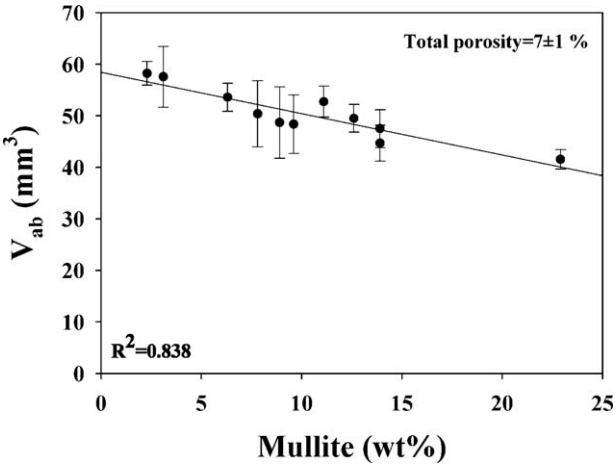

Fig. 9. Volume of material removed by deep abrasion (V_{ab}) as a function of wt% mullite in the fired body. All samples have a porosity of ca. 7 ± 1% and contain mostly closed porosity.

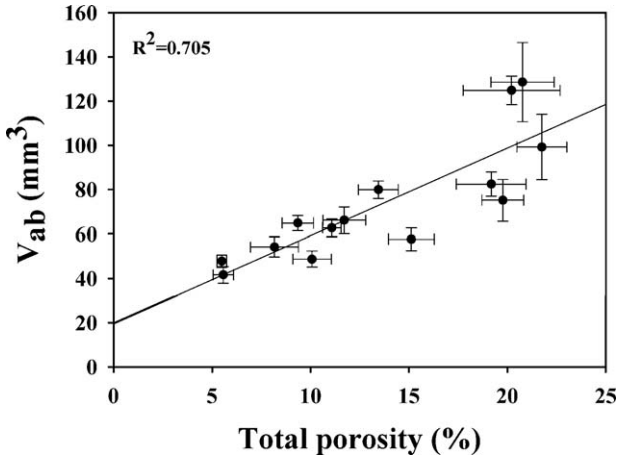

Fig. 10. Volume of material removed by deep abrasion (V_{ab}) as a function of total porosity (TP) for samples with a glass content <ca. 66 wt%.

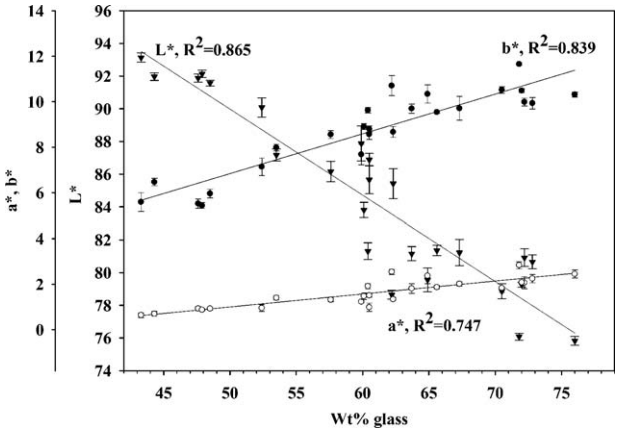

Fig. 12. CIE-Lab colour parameters (L^*, a^* and b^*) as a function of wt% glass in the fired body.

(compare with Fig. 4). When the glass content is higher than ca. 68% (i.e. zone 1), ΔE^* does not change as a function of glass content. This is readily explained by considering Fig. 4 where the total porosity is plotted as a function of glass content. When the glass content is higher than about 66%, the body is fully sintered, i.e. only closed porosity contributes to total porosity. Hence, the pigment cannot enter the sample via interconnected pores at high glass content. Fig. 7 shows top and side view BSE images of samples from mixtures 7 (a and b) 15 (c and d), and 3 (e and f), belonging to zone 1, 2 and 3, respectively. The sample prepared using mixture 7 has a glass content of 76 wt%, and should thus be free of connected pores (see Figs. 4 and 6), which indeed is confirmed by the BSE images of this sample (see Fig. 7a and b). Only large spherical closed pores may be observed. The sample prepared using mixture 15 has a glass content of 63.7%, thus belonging to zone 2. However, although the total porosity of this sample is very similar to the one found for the sample prepared from mixture 7, the degree of staining is higher (33, compared to 2 for sample from mixture 7). In fact, this sample has some interconnected pores which may absorb the staining agent with an increased value of ΔE^* as a result. The sample prepared using mixture 3 has a very low glass content (47.9 wt%) and belongs to zone 3. The value of ΔE^* for this sample is in fact high (56), thus indicating a high density of open pores which is confirmed by the BSE images of this sample (Fig. 7e and f). It can be concluded that connected pores, such as those found in samples from mixture 15 and 3 are detrimental for the resistance to staining. Instead, closed pores as those found in sample 7 have less influence.

3.4.3. Material removed by deep abrasion (V_{ab})

Fig. 8 shows the constant contour plots at low (0 wt%) and high (25 wt%) concentration of added quartz sand for V_{ab}. From the figure, the positive effect of quartz on V_{ab} is quite evident. At low quartz-content, no conclusions can be drawn regarding raw material effects as the variations in V_{ab} are within the model prediction error. At high quartz content, the volume of material removed by deep abrasion (V_{ab}) decreases with increasing proportions of feldspar. Oppositely, kaolin has a positive effect on V_{ab}. These trends are quite similar as the ones observed for porosity. Recent tribological and microstructural studies of porcelain stoneware showed that the porosity and the mullite content were important in determining the amount of material removed by abrasion.[11,27] In order to further investigate the effect of porosity and mineralogical composition on volume

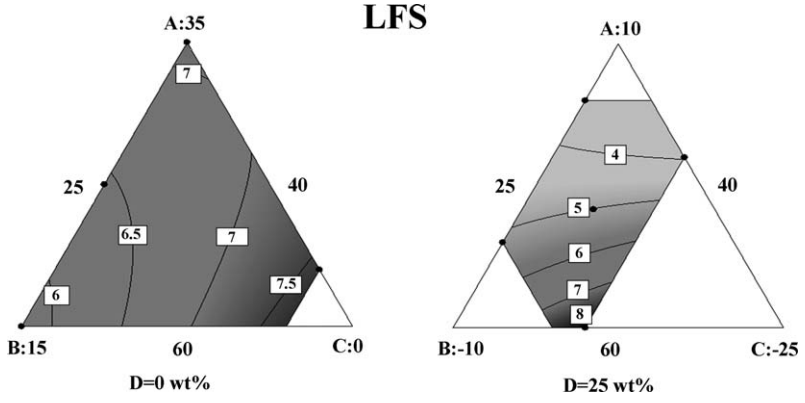

Fig. 11. Constant contour plots at low (0 wt%) and high (25 wt%) percentage of quartz sand for linear firing shrinkage (LFS, %). The raw material codes A, B, C and D correspond to feldspar, kaolin, kaolinitic-illitic clay and quartz sand, respectively.

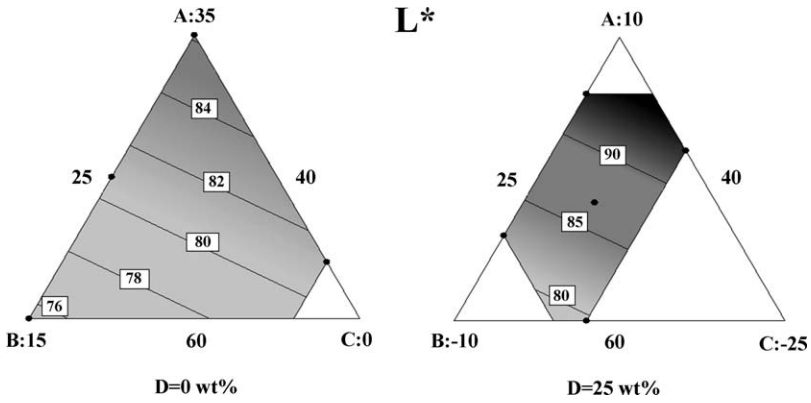

Fig. 13. Constant contour plots at low (0 wt%) and high (25 wt%) percentage of quartz sand for L^*. The raw material codes A, B, C and D correspond to feldspar, kaolin, kaolinitic-illitic clay and quartz sand, respectively.

of material removed by deep abrasion, Fig. 4 is reconsidered in which total porosity is plotted as a function of glass content. At glass content higher than ca. 66 wt%, the total porosity is independent of glass content and remains in the approximate range $7 \pm 1\%$. In these samples, it is likely that closed porosity is the main factor contributing to total porosity (see previous discussion regarding Fig. 4). However, a closer look at the volume removed by deep abrasion for these samples (see Table 3) shows a significant variation which could possibly be explained by the difference in mineralogical composition. In fact, plotting V_{ab} as a function of mullite content results in a negative linear correlation, see Fig. 9. Hence, fully sintered samples with similar values of total porosity may show different resistance to deep abrasion possibly due to differences in phase composition, as found by others.[5,27] Decreasing the glass content below ca. 66 wt% gradually increases the open porosity (Fig. 4). Plotting the material removed by deep abrasion as a function of total porosity results in a positive linear trend, see Fig. 10. Hence, open porosity significantly contributes to decrease the wear resistance. This interpretation is in concert with the conclusions drawn by Martín-Márquez et al. who studied the effect of microstructure on the mechanical properties of porcelain stoneware.[25] They found that the bending strength decreases and increases with open porosity and mullite content, respectively.

3.4.4. Linear firing shrinkage (LFS)

Fig. 11 shows the constant contour plots for the linear firing shrinkage (LFS) at low (0 wt%) and high (25 wt%) concentration of quartz sand. LFS tends to increase with increasing proportions of kaolin and feldspar at low and high quartz-content, respectively, in agreement with previous work.[40] These results are explained by a higher degree of vitrification promoted by feldspar and a higher degree of sintering prompted by kaolinite. In fact, the linear correlation coefficient between LFS and the wt% glass is 0.602 (<0.2% probability that the two variables are uncorrelated[46]) which further highlights the important influence of feldspar on LFS. Quartz sand has a negative effect on the linear firing shrinkage, as expected.

3.4.5. Lab colour parameters (L^*, a^*, b^*)

The specific colour, defined by the CIE-Lab colour parameters, is clearly changing with composition, see Table 3. Positive values for a^* and b^* is observed, demonstrating that the colour is towards red and yellow. Fig. 12 shows the colour parameters as a function of wt% glass in the fired body. Increasing the glass content results in a darker and more coloured body. Sanchez et al. found a linear increase and decrease of L^* and b^*, respectively, with the wt% of crystalline phases (mullite + quartz) in fast-fired porcelain stoneware tiles.[26] The authors attributed these observations with the opacifying effect of the crystalline phases, but pointed out that other mechanisms also could contribute to an increased whiteness such as accommodation of Fe^{3+} in the structure of mullite as well as the presence of pores which also contributes to increasing the whiteness. In this work, we have observed that the mullite structure crystallised in our system does not contain iron. Instead, iron is present in the form of hematite (see Table 5). The surface iron in hematite changes from six to fourfold coordination in contact with the alkaline glass matrix, thus giving a dark brown colour.[57] This is probably the main mechanism governing the change in colour in our system. In fact, increasing the glass content increases the contact surface between the liquid melt and the hematite particles, thus increasing the CIE-Lab parameters a^* and b^*.

Fig. 13 shows the constant contour plots at low (0 wt%) and high (25 wt%) concentration of added quartz sand for the whiteness, L^*. The whiteness decreases with increasing feldspar content whereas kaolin and quartz has a positive effect on this property. The effect of the latter two parameters is possibly related to their positive effect on total porosity and quantity of crystalline phases (mullite and quartz) which both have a positive effect on the whiteness of the ceramic body as a whole.

4. Conclusion

In the present work, the effects of the raw material proportions on the mineralogical composition and various technological properties of porcelain stoneware tiles were investigated using mixture design and statistical modeling in combination with microstructural studies by various techniques such as XRPD

data and Rietveld refinements. The aim was to contribute to the full understanding of this important ceramic system which, due to the high complexity, is not yet reached. The investigated properties were total porosity, linear firing shrinkage, stain resistance, resistance to deep abrasion, CIE-Lab colour parameters (a^*, b^* and L^*) whiteness and bulk density. The following conclusions could be drawn regarding the system studied here:

(i) Based on the refined unit cell parameters, the overall chemical composition of mullite was approximated to $3Al_2O_3{\cdot}2SiO_2$ which is the so-called stoichiometric isomorph. In addition, no evidence was found for the presence of structural Fe in newly formed mullite. The crystallization of mullite from kaolinite was highly governed by the chemical composition of the liquid melt as the fraction of kaolinite transformed into mullite varied between 23 and 45 wt% from low to high kaolinite content.
(ii) A fixed amount of quartz (10 wt% of the dry body weight) was engulfed by the liquid melt during firing, regardless of the initial amount in the raw materials mixture. This indicates saturation of the surrounding melt, i.e. the dissolution of the quartz crystals was controlled by their chemical environment.
(iii) Bulk density was strictly correlated to total porosity.
(iv) The weight fraction of amorphous phase in the stoneware, and consequently the weight fraction of flux in the raw materials mixture, was the most important factor governing the properties of the stoneware: (a) open porosity, and consequently the amount of staining agent retained by the surface (quantified by ΔE^*) decrease linearly with the amount of amorphous phase in the stoneware. A minimum of about 66–68 wt% of amorphous phase is needed to minimize open porosity and thus obtain maximum stain resistance: (b) material removed by deep abrasion is positively dependent on open porosity, and thus amorphous content. In fully sintered samples, i.e. samples having an amorphous content higher than 66–68 wt%, a negative correlation exists between volume removed by deep abrasion and mullite content, thus supporting the mullite hypothesis as a mechanism of strengthening of porcelain stoneware: (c) the CIE-Lab colour parameters a^* and b^* increased with increasing amount of amorphous phase. Instead, a decrease in the whiteness (L^*) with amorphous phase was observed. The increase in a^* and b^* with glass content was attributed to a change from six to fourfold coordination of surface iron in hematite, due to contact with the alkaline glass matrix. A positive effect of kaolin and quartz on whiteness was observed, and possibly related to their positive effect on total porosity and quantity of crystalline phases (mullite and quartz) which both increase the opacity of the ceramic body.

Acknowledgement

P. Miselli, M. Hanuskova and A. Vaccaro are kindly acknowledged for help in the laboratory.

References

1. Sánchez E, García-Ten J, Sanz V, Moreno A. Porcelain tile: almost 30 years of steady scientific–technological evolution. *Ceram Int* 2010;**36**:831–45.
2. Gualtieri AF, Tartaglia A. Thermal decomposition of asbestos and recycling in traditional ceramics. *J Eur Ceram Soc* 2000;**20**:1409–18.
3. Kumar S, Singh KK, Ramachandrarao P. Effects of fly ash additions on the mechanical and other properties of porcelainised stoneware tiles. *J Mater Sci* 2001;**36**:5917–22.
4. Matteucci F, Dondi M, Guarini G. Effect of soda-lime glass on sintering and technological properties of porcelain stoneware tiles. *Ceram Int* 2002;**28**:873–80.
5. Souza GP, Rambaldi E, Tucci A, Esposito L, Lee WE. Microstructural variation in porcelain stoneware as a function of flux system. *J Am Ceram Soc* 2004;**87**:1959–66.
6. Tucci A, Esposito L, Rastelli E, Palmonari C, Rambaldi E. Use of sodalime scrap-glass as a fluxing agent in a porcelain stoneware tile mix. *J Eur Ceram Soc* 2004;**24**:83–92.
7. Luz AP, Ribeiro S. Use of glass waste as a raw material in porcelain stoneware tile mixtures. *Ceram Int* 2007;**33**:761–5.
8. Andreola F, Barbieri L, Karamanova E, Lancellotti I, Pelino M. Recycling of CRT panel glass as fluxing agent in the porcelain stoneware tile production. *Ceram Int* 2008;**34**:1289–95.
9. Souza GP, Messer PF, Lee WE. Effect of varying quartz particle size and firing atmosphere on densification of brazilian clay-based stoneware. *J Am Ceram Soc* 2006;**89**:1993–2002.
10. Leonelli C, Bondioli F, Veronesi P, Romagnoli M, Manfredini T, Pellacani GC, et al. Enhancing the mechanical properties of porcelain stoneware tiles: a microstructural approach. *J Eur Ceram Soc* 2001;**21**:785–93.
11. Tenorio Cavalcante PM, Dondi M, Ercolani G, Guarini G, Melandri C, Raimondo M, et al. The influence of microstructure on the performance of white porcelain stoneware. *Ceram Int* 2004;**30**:953–63.
12. Tucci A, Esposito L, Malmusi L, Rambaldi E. New body mixes for porcelain stoneware tiles with improved mechanical characteristics. *J Eur Ceram Soc* 2007;**27**:1875–81.
13. Zanelli C, Baldi G, Dondi M, Ercolani G, Guarini G, Raimondo M. Glass-ceramic frits for porcelain stoneware bodies: effects on sintering, phase composition and technological properties. *Ceram Int* 2008;**34**:455–65.
14. Gualtieri AF. Thermal behavior of the raw materials forming porcelain stoneware mixtures by combined optical and in situ X-ray dilatometry. *J Am Ceram Soc* 2007;**90**:1222–31.
15. Sánchez E, Ibáñez MJ, García-Ten J, Quereda MF, Hutchings IM, Xu YM. Porcelain tile microstructure: implications for polished tile properties. *J Eur Ceram Soc* 2006;**26**:2533–40.
16. Esposito L, Tucci A, Naldi D. The reliability of polished porcelain stoneware tiles. *J Eur Ceram Soc* 2005;**25**:1487–98.
17. Dondi M, Ercolani G, Guarini G, Melandri C, Raimondo M, Rocha e Almendra E, et al. The role of surface microstructure on the resistance to stains of porcelain stoneware tiles. *J Eur Ceram Soc* 2005;**25**:357–65.
18. Cannillo V, Esposito L, Rambaldi E, Sola A, Tucci A. Effect of porosity on the elastic properties of porcelainized stoneware tiles by a multi-layered model. *Ceram Int* 2009;**35**:205–11.
19. De Noni Jr A, Hotza D, Cantavella Soler V, Sánchez Vilches E. Influence of composition on mechanical behaviour of porcelain tile. Part I: Microstructural characterization and developed phases after firing. *Mater Sci Eng* 2010;**527**:1730–5.
20. De Noni Jr A, Hotza D, Cantavella Soler V, Sánchez Vilches E. Influence of composition on mechanical behaviour of porcelain tile. Part II: Mechanical properties and microscopic residual stress. *Mater Sci Eng* 2010;**A527**:1736–43.
21. Amorós JL, Orts MJ, García-Ten J, Gozalbo A, Sánches E. Effect of the green porous texture on porcelain tile properties. *J Eur Ceram Soc* 2007;**27**:2295–301.
22. Mukhopadhyay TK, Ghatak S, Maiti HS. Effect of pyrophyllite on the mullitization in triaxial porcelain system. *Ceram Int* 2009;**35**:1493–500.
23. Carbajal L, Rubio-Marcos F, Bengochea MA, Fernandez JF. Properties related phase evolution in porcelain ceramics. *J Eur Ceram Soc* 2007;**27**:4065–9.

24. Martín-Márquez J, Ma Rincón J, Romero M. Effect of firing temperature on sintering of porcelain stoneware tile. *Ceram Int* 2008;**34**:1867–73.
25. Martín-Márquez J, Ma Rincón J, Romero M. Effect of microstructure on mechanical properties of porcelain stoneware. *J Eur Ceram Soc* 2010;**30**:3063–9.
26. Sanchez E, Orts MJ, Garcia-Ten J, Cantavella V. Porcelain tile composition effect on phase formation and end products. *Am Ceram Soc Bull* 2001;**80**:43–9.
27. Dondi M, Guarini G, Melandri C, Raimondo M, Tenerio Cavalcante PM, Zanelli C. Resistance to deep abrasion of porcelain stoneware tiles: key factors. *Ind Ceram* 2005;**25**:71–8.
28. Martín-Márquez J, De la Torre AG, Aranda MAG, Ma Rincón J, Romero M. Evolution with temperature of cristalline and amorphous phases in porcelain stoneware. *J Am Ceram Soc* 2009;**92**:229–34.
29. Gualtieri AF, Zanni M. Quantitative determination of crystalline and amorphous phases in traditional ceramics by combined Rietveld-RIR method. *Mater Sci Forum* 1998;**278–281**:834–9.
30. Gualtieri AF. Accuracy of XRPD QPA using the combined Rietveld-RIR method. *J Appl Cryst* 2000;**33**:267–78.
31. Ferrari S, Gualtieri AF. The use of illitic clays in the production of stoneware tile ceramics. *Appl Clay Sci* 2006;**32**:73–81.
32. Eriksson L, Johansson E, Wikström C. Mixture design-design generation, PLS analysis, and model usage. *Chemometr Intell Lab Syst* 1998;**43**:1–24.
33. Box GEP, Hunter WG, Hunter JS. *Statistics for experimenters*. New York: Wiley; 1978.
34. Romagnoli M, Rivasi MR. Optimal size distribution to obtain the densest packing: a different approach. *J Eur Ceram Soc* 2007;**27**:1883–7.
35. Correia SL, Grun E, Denardi CD, Hotza D, Folgueras MV. Effects of raw materials on the technological properties of brick compositions using a statistical design approach. *Mater Sci Forum* 2006;**530–531**:486–91.
36. Lever DA. Optimisation of ceramic systems using experimental design and modeling. In: Vincenzini P, Dondi M, editors. *Proceedings of the international conference science for new technology of silicate ceramics*. 2003. p. 17–24.
37. Pham-Gia K, Melchner R, Mörtel H, Voit K. Application of laser scanning microscopy in the development of highly abrasion-resistant glazes for fast-fired hard paste porcelain. *Ceram Forum Int* 2001;**78**:E34–9.
38. Poyraz HB, Erginel N, Ay N. The use of pumice (pumicite) in transparent roof tile glaze composition. *J Eur Ceram Soc* 2006;**26**:741–6.
39. Cabrelon MD, Zauberas RT, Melchiades FG, Boschi AO. Design of experiments with mixture variables as a tool for the formulation of pigments: the case of the blue (V–$ZrSiO_4$). *Ceram Forum Int* 2006;**83**. p. E41–E46, D31.
40. Correia SL, Hotza D, Segadães AM. Simultaneous optimization of linear firing shrinkage and water absorption of triaxial ceramic bodies using experiments design. *Ceram Int* 2004;**30**:917–22.
41. Correia SL, Oliveira APN, Hotza D, Segadães AM. Properties of triaxial porcelain bodies: interpretation of statistical modeling. *J Am Ceram Soc* 2006;**89**:3356–65.
42. Bernardin AM, de Medeiros DS, Riella HG. Pyroplasticity in porcelain tiles. *Mater Sci Eng* 2006;**A427**:316–9.
43. Menezes RR, Malzac Neto HG, Santana LNL, Lira HL, Ferreira HS, Neves GA. Optimization of wastes content in ceramic tiles using statistical design of mixture experiments. *J Eur Ceram Soc* 2008;**28**: 3027–39.
44. Larson AC, Von Dreele RB. *GSAS generalized structure analysis system. Laur 86-748*. Los Alamos: Los Alamos National Laboratory; 1994.
45. Toby BH. EXPGUI, a graphical user interface for GSAS. *J Appl Cryst* 2001;**34**:210–3.
46. Taylor Jr. *An introduction to error analysis, the study of uncertainties in physical measurements*. 2nd ed. USA: University Science Books; 1997.
47. Ban T, Okada K. Structure refinement of mullite by the Rietveld method and a new method for estimation of chemical composition. *J Am Ceram Soc* 1992;**75**:227–30.
48. Cameron WE. Composition and cell dimensions of mullite. *Am Ceram Soc Bull* 1977;**56**:1003–11.
49. Iqbal Y, Lee WE. Fired porcelain microstructures revised. *J Am Ceram Soc* 1999;**82**:3584–90.
50. Ocaña M, Caballero A, González-Carreño T, Serna CJ. Preparation by pyrolysis of aerosols and structural characterization of Fe-doped mullite powders. *Mater Res Bull* 2000;**35**:775–88.
51. Paganini A, Francescon F, Pavese A, Diella V. Sanitary-ware vitreous body characterization method by optical microscopy, elemental maps, image processing and X-ray powder diffraction. *J Eur Ceram Soc* 2010;**30**:1267–75.
52. Lee WE, Souza GP, McConville CJ, Tarvornpanich T, Iqbal Y. Mullite formation in clays and clay-derived vitreous ceramics. *J Eur Ceram Soc* 2008;**28**:465–71.
53. Gualtieri A, Bellotto M, Artioli G, Clark SM. Kinetic study of the kaolinite-mullite reaction sequence. Part II: Mullite formation. *Phys Chem Miner* 1995;**22**:215–22.
54. Vogel W. *Chemistry of glass*. OH: The American Ceramic Society Inc.; 1985.
55. Suvaci E, Tamsu N. The role of viscosity on microstructure development and stain resistance in porcelain stoneware tiles. *J Eur Ceram Soc* 2010;**30**:3071–7.
56. Lakatos T, Johansson L-G, Simmingsköld B. Viscosity temperature relations in the glass system SiO_2–Al_2O_3–Na_2O, K_2O, CaO, MgO in the composition range of technical glasses. *Glass Technol* 1972;**13**:88–95.
57. Gualtieri AF. Development of low-firing B-fluxed stoneware tiles. *J Am Ceram Soc* 2009;**92**:2571–7.